Design, Parameters, and Tolerances for the LCLS First Bunch Compressor Chicane, 'BC1'

P. Emma
SLAC

October 7, 2004

ABSTRACT

This note describes the details of the LCLS BC1 first-stage bunch compressor chicane design, including installation issues; diagnostics; vacuum chamber impedance; system tuning; and tolerances on field quality, alignment, and regulation of the dipole magnets.

1 Introduction

The electron bunch from the LCLS RF photocathode gun is compressed from 830 μm to 195 μm in this first stage of compression, called the BC1 chicane. This note describes the details of the chicane design, including installation issues; diagnostics; vacuum chamber impedance; system tuning; and tolerances on field quality, alignment, and regulation of the dipole magnets.

2 Chicane Design Requirements

The design of the chicane and its location are set by the following goals:

- The chicane should generate a momentum compaction ($|R_{56}|$) which ranges from 15 to 65 mm at a nominal electron energy of 250 MeV.
- The chicane bends should not increase the normalized horizontal projected emittance ($\gamma\varepsilon_{x_0} \approx 1$ μm) by more than about 10%.
- The chicane should include beam energy and energy spread diagnostics at its center (BPM and profile monitor) as well as 2 independently adjustable horizontal collimator jaws.
- It should be possible to switch off the chicane for non-compressed operations to pass the 30-GeV test beams.
- The chicane is to be located at the 21-2 location in the SLAC linac.

Since the chicane must be switched off and straightened out for 30-GeV test beams in the linac, and also requires a high resolution BPM at its center, it has been determined that the center two magnets will be placed on a horizontal translation stage and remotely moved in synchronization with the dipole field settings.

3 Chicane Location and Parameters

A simple 4-dipole chicane is shown in Figure 1, with some symbol definitions used below. It is composed of rectangular bends with no magnet yaw as in Figure 1. Two small ‘tweaker’ quadrupole magnets are included to allow fine tuning of the final suppressed dispersion. These quadrupoles are nominally set to zero field gradient.

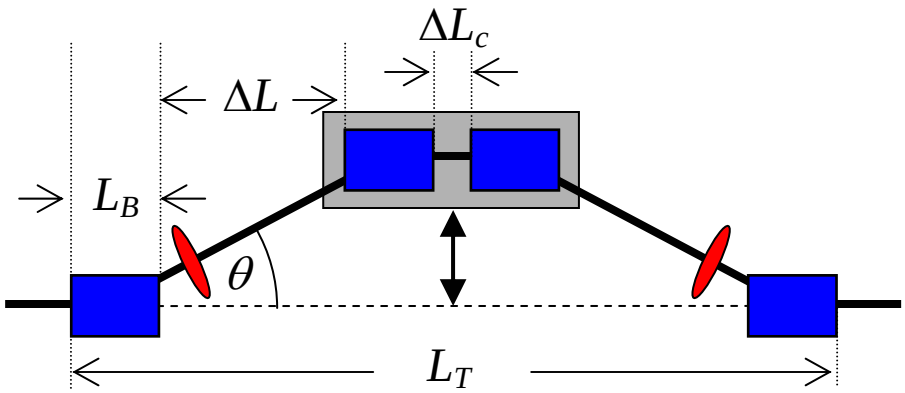

Figure 1. Four-dipole chicane with symbol definitions, parallel (un-yawed) magnets, 'tweaker' quadrupoles, and a moveable translation stage supporting the center two magnets to allow straightening the chicane.

The 4-dipole chicane's ability to compress the bunch is its momentum compaction, which is given approximately (for $\theta << 1$) by

$$R_{56} \approx -2\theta^2\left(\Delta L + \frac{2}{3}L_B\right), \tag{1}$$

where the symbols are taken from Figure 1 (bunch head defined at $z < 0$). The bend-plane emittance growth due to incoherent synchrotron radiation is given by [1]

$$\Delta\gamma\varepsilon_x \approx \left(8\times10^{-8}\ \mathrm{m^2\cdot GeV^{-6}}\right)\cdot E^6\frac{\left|\theta^5\right|}{L_B^2}\left(\Delta L + L_B + \frac{\breve{\beta}+\hat{\beta}}{3}\right), \tag{2}$$

where the minimum, $\breve{\beta}$, and maximum, $\hat{\beta}$, beta-function values in the chicane are included, and E is the electron energy [1].

At $E = 250$ MeV, the emittance growth is negligible. The net chicane length is $L_T = 6.5128$ m (from start of 1st effective bend to end of 4th effective bend), includes a $\Delta L_c = 0.830$-m drift between bend-2 and bend-3 to allow placement of a beam position monitor (BPM), profile monitor, and collimator.

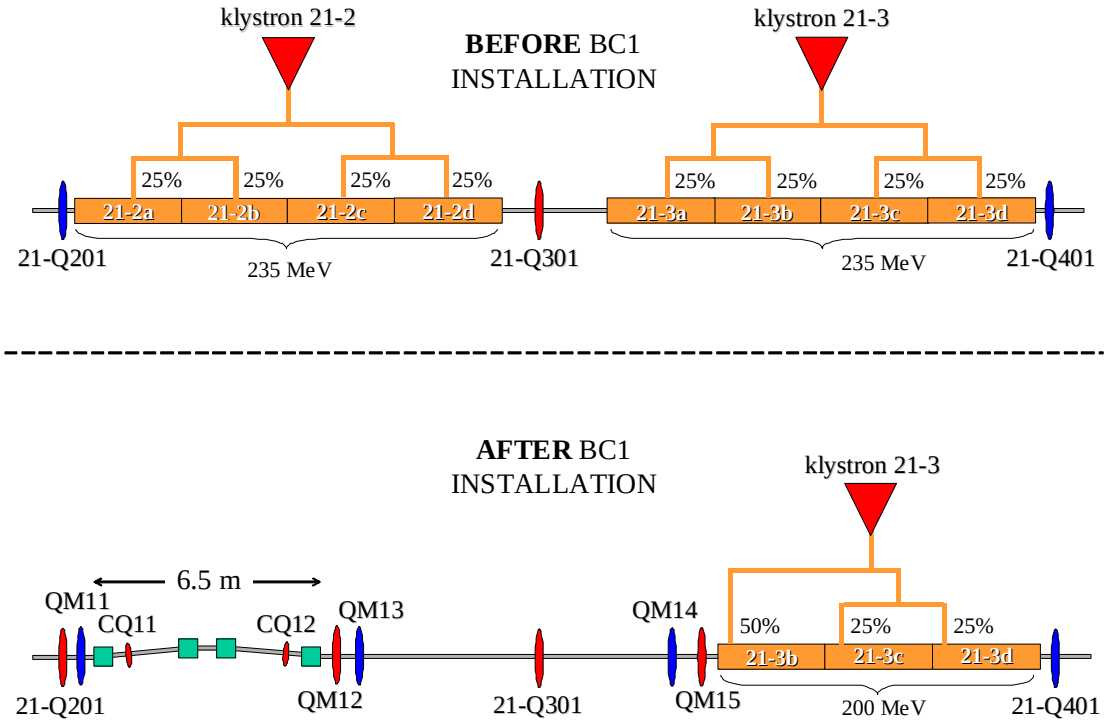

Figure 2. Schematic of linac at sector 21-2 and 21-3 showing layout and klystron configuration both before (top) and after (bottom) BC1 chicane installation.

This placement provides >15 meters of space for the chicane and a permanent linac energy loss of 270 MeV. Figure 2 shows the layout in this area both before and after BC1 chicane installation. The chicane parameters are listed in Table 1.

Table 1. Four-dipole chicane parameters at the sector 21-2 location.

parameter	**symbol**	**value**	**unit**
electron energy	E	250	MeV
linear rms energy spread for min. compression	σ_δ	1.6	%
momentum compaction	R_{56}	–39.0	mm
bend angle per dipole	$\|\theta\|$	4.971	deg
effective length of each dipole magnet *	L_B	0.2032	m
drift length between bend-1(3) and bend-2(4) *	ΔL	2.4349	m
drift length between bend-2 and bend-3	ΔL_c	0.830	m
total chicane length	L_T	6.513	m
bend radius per dipole	$\|\rho\|$	2.345	m
field of dipole magnets	$\|B_0\|$	3.556	kG
peak dispersion (= maximum chicane deflection)	η_{pk}	0.229	m

* Measured along straight linac axis, not along curved axis of beam

Correction quadrupoles, CQ11 and CQ12, have been added inside the chicane to provide empirical tuning of anomalous linear dispersion after the chicane. Their specifications are described below in the tuning section.

The beta functions in the sector 21-2 area after chicane installation are shown in Figure 3. A block layout is shown above these plots.

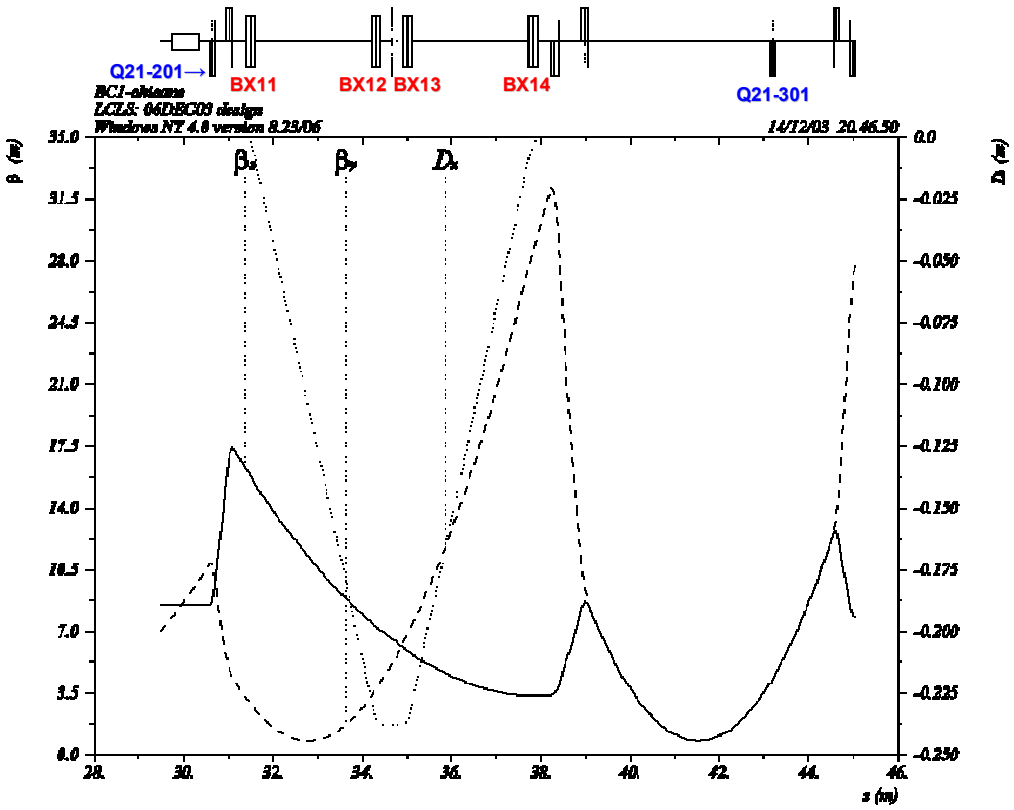

Figure 3. Linac sector 21-2 and 21-3 after BC1 chicane installation, where accelerating sections 21-2a,b,c,d and 21-3a have all been removed (not precisely to scale here).

4 Tuning of the Compressor

It will be useful to vary the compression factor over a small range in order to accommodate uncertainties in the beam dynamics. Ideally, the compression factor would be variable from $R_{56} = 0$, to well beyond nominal (*e.g.*, $R_{56} \approx -65$ mm). This, however, requires very wide magnet apertures to accommodate the off-axis beam and also demands a very flat field over a very large width (>0.4 m in this ideal case). It is best to move the inner magnets horizontally on a translation stage. The horizontal translation range of the center bends then extends from zero (dipoles off) out to 0.296 m, with a nominal offset of

0.229 m. The bend fields must then operate between zero and 5.5 kG to allow $|R_{56}|$ up to 65 mm and a top end energy of 300 MeV.

Correction quadrupoles, CQ11 and CQ12, have been added inside the chicane to provide empirical tuning of anomalous linear dispersion after the chicane (see Figure 2). These have nominal strength of zero (for the four-dipole chicane of Figure 1), but can be used to minimize the horizontal emittance after the chicane. (Emittance measuring wire-scanners will be located in sector-21-3, just after the chicane.) The small tuning quadrupole magnets are, for example, 0.1-m long with a 15-mm radius and pole-tip field capability of ±0.10 kG, and are located 0.3-m inboard of the B1 and B4 dipole magnets (see Figure 2). The nominal horizontal beam size in these tuner quadrupoles is 0.62 mm rms ($\eta_x \approx 39$ mm, $\langle \delta^2 \rangle^{1/2} \approx 1.6$ %), and is completely dominated by dispersion, so their effect on beta functions is much less significant.

5 Aperture and Field Quality

The dipole magnets will include separate trim coils which can adjust the dipole field by up to approximately ±1 %. These will be on bipolar power supplies and used to equalize the measured dipole fields over the four magnets and may also be used for horizontal trajectory correction, especially when the chicane is switched off and the remnant field must be compensated. The integrated field strength of each dipole magnet must be constant over the four magnets to a level of $|\Delta B/B_0| < 0.1\%$.

The very large horizontal beam size within the chicane (up to 5 mm rms) makes the aperture and field quality tolerances quite demanding. This is especially true considering the curved path which the beam follows through the rectangular bends (see Figure 4).

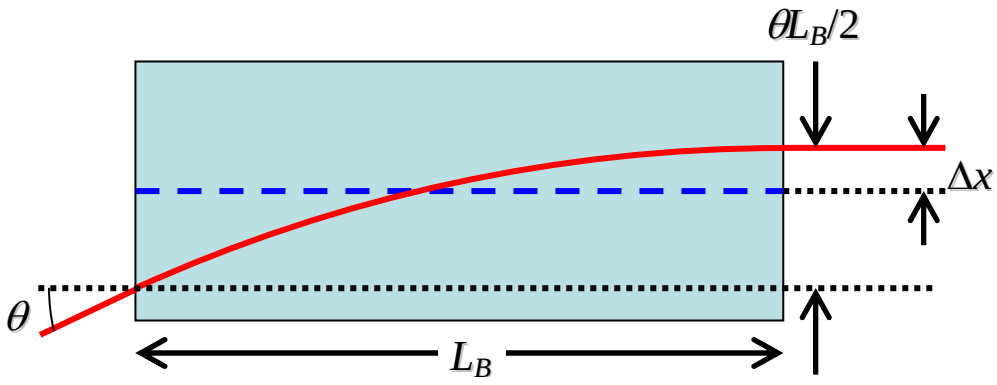

Figure 4. Curved path through bend with intentional magnet offset, Δx.

The full width traced by the beam through the magnet is $\zeta \approx \theta L_B/2$. The full aperture width required in the inner bends, w, is then given in terms of the beam size ($\eta_{pk} \approx -\theta\{\Delta L + L_B\}$), and the width ζ, or

$$w \geq \frac{\theta L_B}{2} + 20\sigma_\delta \left|\eta_{pk}\right|. \tag{3}$$

This provides ±10-sigma beam-size clearance, plus space for the curved trajectory. With the parameters of Table 1, the *minimum* full-width horizontal aperture is $w \approx 10$ cm (3.9 inches). The outer magnets do not need so much aperture ($w_{\text{outer}} > 2$ cm), but identical magnets are simpler to fabricate.

The field quality over these widths should be very flat in order not to generate residual momentum dispersion of 1st or higher order. The field quality tolerance can be estimated by assuming a dipole field which includes some sextupole component (field dependence with x^2).

$$\frac{\Delta B_y(x,y)}{B_y(0,0)} = \frac{b_2}{b_0}\frac{x^2 - y^2}{r_0^2} \tag{4}$$

Here, r_0, is the reference radius (*e.g.*, the probe radius used to measure the field), and b_2/b_0 is the length-integrated relative sextupole field component of the magnet. The horizontal beam position and size is typically well dominated by the bending and energy spread, so the betatron component of the trajectory in x and y can be ignored.

5.1 Outer Dipoles

The horizontal beam trajectory in the first or last bend follows the Figure 4 curve,

$$x \approx \frac{\theta L_B}{2}\left(\frac{s}{L_B}\right)^2 (1-\delta) + \Delta x\,, \tag{5}$$

where $\delta\,(\equiv \Delta E/E_0)$ is the relative energy deviation from nominal, s is the distance traveled along the bend magnet ($s = 0$ at entrance), and Δx is a possible misalignment. Equation (5) is substituted into (4) and the kick angle *error*, $\Delta x'$, accumulated as the beam moves farther off in the sextupole field, is integrated along s. The angle error is dominant, while the spatial error at the end of the magnet, Δx, is ignored.

$$\Delta x' = \frac{1}{(B\rho)}\int_0^{L_B}\Delta B_y\,ds = \left(\frac{b_2}{b_0}\right)\frac{\theta}{L_B r_0^2}\int_0^{L_B} x^2\,ds \tag{6}$$

Here ($B\rho$) is the standard magnetic rigidity, and the kick error, $\Delta x'$, is zero if the sextupole component is zero. With a significant sextupole field, an effective emittance growth is generated as the horizontal beam size extends over an effective field gradient which gets steeper as the beam is forced farther off axis. The net effect is to generate residual linear dispersion after the chicane.

The associated emittance growth can be estimated by taking the ensemble average of the particle kicks $\langle \Delta x'^2 \rangle$ and using $\Delta\varepsilon_x/\varepsilon_{x0} \approx 0.5\langle \Delta x'^2\rangle \beta_x/\varepsilon_{x_0} << 1$, where β_x is the beta function at the dipole centers,

$$\frac{\Delta\varepsilon_x}{\varepsilon_{x_0}} \approx \frac{1}{18}\left(\frac{b_2}{b_0}\right)^2 \theta^4 \sigma_\delta^2 \frac{\beta_x}{\varepsilon_{x_0}} \frac{L_B^2}{r_0^4}\left(\frac{3}{10}\theta L_B - \Delta x\right)^2 , \tag{7}$$

and $\sigma_\delta \equiv \langle(\delta - \langle\delta\rangle)^2\rangle^{1/2}$ is the relative rms energy spread in the incoming beam. The mean kick angle, $\langle \Delta x' \rangle$, has been subtracted in Eq. (7), since it is simply a steering effect. The emittance effect can be negated by moving the dipole transversely, away from the linac axis, by $\Delta x = 3\theta L_B/10 \approx 5.0$ mm (as in Figure 4).

The effect described above is a sextupole 'feed-down', and without the proper value of Δx, is completely equivalent to a linear dispersion error at the end of the chicane. It can be empirically corrected with the CQ11 and CQ12 quadrupoles in the chicane.

5.2 Inner Dipoles

This effect can be calculated for the inner two dipoles by including the large peak dispersion function in the center of the chicane, $\eta_{pk} \approx -\theta(L_B + \Delta L)$. The energy dependent trajectory is rewritten to include the peak dispersion as

$$x \approx \frac{\theta L_B}{2}\left[\left(\frac{s}{L_B}\right)^2 - 2\frac{s}{L_B} + 1 + \frac{2\eta_{pk}}{\theta L_B}\right]\delta - \frac{\theta L_B}{2}\left[\left(\frac{s}{L_B}\right)^2 - 2\frac{s}{L_B} + 1\right] + \Delta x , \tag{8}$$

and the integral over x^2 is evaluated as in Eq. (6). The emittance growth for one of the inner bends is then given by

$$\frac{\Delta\varepsilon_x}{\varepsilon_{x_0}} \approx \frac{1}{18}\left(\frac{b_2}{b_0}\right)^2 \theta^4 \sigma_\delta^2 \frac{\beta_x}{\varepsilon_{x_0}} \frac{L_B^2}{r_0^4}\left(6\left|\frac{\eta_{pk}}{\theta L_B}\right|-1\right)^2 \left\{\Delta x - \frac{3}{10}\theta L_B\left(\frac{\frac{10}{3}\left|\frac{\eta_{pk}}{\theta L_B}\right|-1}{6\left|\frac{\eta_{pk}}{\theta L_B}\right|-1}\right)\right\}^2 , \qquad (9)$$

which can be reduced to zero by misaligning the bends toward the linac axis by

$$\Delta x = \frac{3}{10}\theta L_B\left(\frac{\frac{10}{3}\left|\frac{\eta_{pk}}{\theta L_B}\right|-1}{6\left|\frac{\eta_{pk}}{\theta L_B}\right|-1}\right), \qquad (10)$$

and amounts to $\Delta x \approx 2.8$ mm for the parameters of Table 1. The actual value of Δx needs to be precise to ±2 mm (2 % emittance growth with $|b_2/b_0| = 0.07$ % at $r_0 = 20$ mm). The emittance growth is, however, correctable with the tuning quadrupoles, CQ11 and CQ12.

With their even larger beam size, however, the inner bends set a critical tolerance on the sextupole component based on the quadratic field variation over the large beam size. This tolerance, for a Gaussian energy spread, is given by

$$\frac{\Delta\varepsilon_x}{\varepsilon_{x0}} \approx \left(\frac{b_2}{b_0}\right)^2 \left(\frac{\eta_x}{r_0}\right)^4 \theta^2 \sigma_\delta^4 \frac{\beta_x}{\varepsilon_{x0}}, \qquad (11)$$

where η_x and β_x are the dispersion and beta functions in the dipole centers. For the inner bends, with $\eta_x \approx 0.231$ m and $\beta_x \approx 7$ m, the tolerance is $|b_2/b_0| < 0.07\%$ at $r_0 = 20$ mm for an emittance growth of 2% in one inner bend. This aberration generates second-order dispersion at the end of the chicane, and is not correctable, unless tuning sextupoles are also included (not planned). *This tolerance is therefore a critical one for the inner bends*. If both inner bends have the same sextupole field, the tolerance is $|b_2/b_0| < 0.05\%$.

5.3 Aperture and Field Quality Summary

Further field tolerances can be calculated which also include quadrupole (x), octupole (x^3), and decapole (x^4) field dependence terms. A summary of field quality tolerances for the inner bends and the outer bends is listed in Table 2, where the critical tolerances (uncorrectable) are listed in **bold** text. These are calculated for a worst case, combined emittance growth of <5%, and verified with particle tracking. The field harmonics are evaluated at a radius $r_0 = 20$ mm with respect to the physical pole center-line of the

rectangular bend magnets. The most challenging tolerance is the sextupole term for the inner bends at $|b_2/b_0| < 0.05\%$ at $r_0 = 20$ mm.

Table 2. Aperture and field quality tolerances for chicane dipole magnets evaluated at a radius $r_0 = 20$ mm. The critical tolerances (uncorrectable) are listed in **bold** text.

parameter	**symbol**	**outer bends**	**inner bends**	**unit**
trim coil adjustability (% of main field)	$(\Delta B/B_0)_{\text{trim}}$	±1	±1	%
minimum physical aperture full-width	w	0.02	0.10	m
max. dipole field error (w.r.t. other bends)	$\lvert\Delta B/B_0\rvert$	0.1	0.1	%
maximum quadrupole field component	$\lvert b_1/b_0\rvert$	0.10/**0.2**	0.01/**0.2**	%
maximum sextupole field component	$\lvert b_2/b_0\rvert$	**1**	**0.05**	%
maximum octupole field component	$\lvert b_3/b_0\rvert$	**2**	**0.1**	%
maximum decapole field component	$\lvert b_4/b_0\rvert$	**5**	**0.2**	%

6 Magnet Alignment and Field Regulation

The field quality requirements are used to set the magnet alignment tolerances by assuming the field quality tolerances are just met. Horizontal misalignments generate horizontal linear dispersion (correctable with the tuner quads), while vertical misalignments generate vertical linear dispersion, which is not easily correctable without skew tuner quadrupoles (not planned). The horizontal, Δx, and vertical, Δy, alignment tolerances of a bend with sextupole relative field component (b_2/b_0), and dispersion dominated beam size, are

$$|\Delta x| < \frac{r_0^2}{\sqrt{2}\left|(b_2/b_0)\theta\eta_x\right|}\frac{\sqrt{\Delta\varepsilon_x/\varepsilon_{x_0}}}{\sigma_\delta}\sqrt{\frac{\varepsilon_{x_0}}{\beta_x}}\,, \tag{12}$$

$$|\Delta y| < \frac{r_0^2}{\sqrt{2}\left|(b_2/b_0)\theta\eta_x\right|}\frac{\sqrt{\Delta\varepsilon_y/\varepsilon_{y_0}}}{\sigma_\delta}\sqrt{\frac{\varepsilon_{y_0}}{\beta_y}}\,, \tag{13}$$

where η_x is the mean dispersion in the bend, $\beta_{x,y}$ is the x or y beta function in the bend ($\beta_x \approx 16$ m, $\beta_y \approx 7$ m), and ε_{x,y_0} is the nominal x or y geometric emittance ($\varepsilon_{x_0} \approx \varepsilon_{y_0} \approx 2\times10^{-9}$ m). For the inner bends, with $(b_2/b_0) \approx 0.05\%$ at $r_0 = 20$ mm and $\Delta\varepsilon_{x_0}/\varepsilon_{x_0} = \Delta\varepsilon_{y_0}/\varepsilon_{y_0} = 1\%$, the alignment tolerances are $|\Delta x| < 2.0$ mm, and $|\Delta y| < 3.0$ mm. The outer bends are much looser. Allowing both inner bends to be misaligned, the alignment tolerances per dipole become $|\Delta x| < 1.4$ mm, and $|\Delta y| < 2.0$ mm.

Magnet roll errors generate vertical dispersion, but this is observable and correctable by local steering. The power supply regulation tolerance is based on one supply feeding all magnets in series. In this case, a lack of regulation causes a 'time-of-flight' error through the chicane and following linac, which should be held to $|\Delta z| < 10$ μm rms (30 fsec).

$$\left|\frac{\Delta B}{B_0}\right| < \left|\frac{\Delta z}{R_{56}}\right| \approx 0.02\% \tag{14}$$

The longitudinal alignment tolerance is estimated by the linear dispersion, and therefore emittance growth, induced with an axial shift of one magnet by Δs.

$$\frac{\Delta\varepsilon_x}{\varepsilon_{x0}} \approx \frac{1}{2}\Delta s^2\theta^2\sigma_\delta^2\frac{\gamma_x}{\varepsilon_{x0}} << 1 \tag{15}$$

Here $\gamma_x \equiv (1 + \alpha_x^2)/\beta_x$ is evaluated after B4 ($\alpha_x \approx 0$, $\beta_x \approx 3.4$ m) and sets a longitudinal alignment tolerance of $|\Delta s| < 5$ mm for an emittance increase of $\Delta\varepsilon_x/\varepsilon_{x_0} \approx 1$ % (the tolerance has been divided by two to accommodate four randomly misaligned dipoles).

Table 3. Magnet alignment and power supply regulation tolerances. The critical tolerances (uncorrectable) are listed in **bold** text.

parameter	**symbol**	**outer bends**	**inner bends**	**unit**
roll angle of each magnet	$\|\phi\|$	**1.0**	**1.0**	mrad
horizontal alignment (for $b_2/b_0 \approx \pm 0.05\%$)	$\|\Delta x\|$	3.0	1.4	mm
vertical alignment (for $b_2/b_0 \approx \pm 0.05\%$)	$\|\Delta y\|$	**3.0**	**2.0**	mm
longitudinal alignment	$\|\Delta s\|$	5.0	5.0	mm
power supply rms regulation tolerance	$\|\Delta B/B_0\|$	**0.02**		%

7 Diagnostics in the Chicane

It will be important to measure the relative energy deviation and the energy spread in the chicane. The relative energy deviation is easily measured by placing a BPM in the center of the chicane. Based on the power supply regulation tolerance in Table 3, the BPM resolution should be $\langle x^2\rangle^{1/2} << \eta_{pk}|\Delta B/B_0| \approx 50$ μm rms. The linear dynamic range should cover at least ± 5 mm to allow an intentional energy variation of $\pm 2\%$ to measure the dispersion.

The relative energy spread will be measured using an retractable screen-type profile monitor to measure the horizontal spot size. The beam size in the center of the chicane is

$\sigma_x \approx |\eta_{pk}|\sigma_\delta \approx 3.8$ mm rms. So the screen should cover a full field of view of $12\sigma_x \approx 45$ mm with a pixel resolution of <100 μm, if possible.

Independently adjustable horizontal collimator jaws should also be included at the center of the chicane. The jaws should withstand the full average beam power (30 watts at $E = 250$ MeV, $Q = 1$ nC and $f = 120$ Hz). The jaws should be adjustable in <100 μm steps, be able to open to ±50mm, and close to within ~100 μm, with the capability to each cross-over the point where $x = 0$.

The sequence order, in the direction of the beam, of the diagnostics in the chicane center should be: BPM, collimator, and then screen.

8 Vacuum Chamber

There are additional requirements on the conductivity of the inner surface of the vacuum chamber and the number of expansion bellows allowed within the chicane. A low conductivity inner surface, or too many bellows convolutions can generate a longitudinal wakefield energy spread within the chicane which can couple into the horizontal plane and degrade the emittance. These wakefields are enhanced as the bunch length is compressed, forcing tighter constraints on the downstream half of the chicane. If the wakefield-induced rms energy spread, σ_{δ_w}, is generated between the 3rd and 4th bends, the longest section where the bunch is fully compressed, the bend-plane emittance growth is approximately

$$\frac{\varepsilon_x}{\varepsilon_{x0}} \approx \sqrt{1+\sigma_{\delta_w}^2\theta^2\frac{\beta_x}{\varepsilon_{x0}}}, \qquad \text{or} \qquad \frac{\Delta\varepsilon_x}{\varepsilon_{x0}} \approx \frac{1}{2}\sigma_{\delta_w}^2\theta^2\frac{\beta_x}{\varepsilon_{x0}} << 1 \quad . \tag{16}$$

With $\beta_x \approx 3.4$ m taken at the center of the 4th bend, $|\theta| \approx 84$ mrad, and $\varepsilon_{x0} \approx 2\times10^{-9}$ m at 250 MeV, a wakefield-induced rms relative energy spread of just $\sigma_{\delta_w} \approx 6\times10^{-5}$ causes a 2% emittance growth in the bend plane.

8.1 Resistive-Wall Wakefields

For a Gaussian temporal bunch shape, a resistive vacuum chamber surface generates an energy spread within the chicane, σ_{δ_w}, according to [2]

$$\sigma_{\delta_w} \approx 0.22\frac{e^2cNL}{\pi^2 aE\sigma_z^{3/2}}\sqrt{\frac{Z_0}{\sigma}}, \qquad \sigma_z \geq s_0 \equiv \left(\frac{2a^2}{Z_0\sigma}\right)^{1/3}, \tag{17}$$

where e is the electron charge, c is the speed of light, N is the bunch population, L is the vacuum chamber length, Z_0 is the free-space impedance (377 Ω), a is the vacuum chamber radius (or half-height), E is the electron energy, σ_z is the rms bunch length, and σ is the conductivity of the inside surface. Equation (15) is an overestimate for bunch lengths which are less than s_0 (note, $\sigma_z > s_0$ in BC1).

The emittance effect ($\Delta\varepsilon_x/\varepsilon_{x0} << 1$) is estimated for the long vacuum chamber between the 3rd and including half the 4th bend, where the bunch is at its shortest for the longest distance. In this case, $L \approx \Delta L + L_B/2 \approx 2.54$ m, and $\sigma_z \approx 190$ μm, while the vacuum chamber is assumed to have a large horizontal width but small vertical dimension of full-height $2a$.

$$\frac{\Delta\varepsilon_x}{\varepsilon_{x0}} \approx 0.024\left[\frac{e^2 cN\left(\Delta L + L_B/2\right)}{\pi^2 aE}\right]^2 \frac{Z_0}{\sigma}\frac{1}{\sigma_z^3}\theta^2\frac{\beta_x}{\varepsilon_{x0}} << 1 \qquad (18)$$

For stainless steel with $\sigma \approx 1.4\times10^6\ \Omega^{-1}\cdot\text{m}^{-1}$, a vacuum chamber full-height of $2a \approx 30$ mm, ($s_0 \approx 95$ μm), $\beta_x \approx 3.4$ m, and $N \approx 6.2\times10^9$, the emittance growth is approximately $\Delta\varepsilon_x/\varepsilon_{x0} \approx 0.5$ %. It is therefore important to keep the vacuum chamber full-height $2a > 30$ mm if the chamber is stainless steel. The upstream vacuum chambers will have much less effect since the bunch length is longer there.

8.2 Vacuum Bellows Wakefields

Discontinuities in the vacuum chambers can also generate energy spread within the chicane and cause bend-plane emittance growth. The rms energy spread generated by a vacuum bellows of total length ℓ, with M closely spaced periodic convolutions, is [3]

$$\sigma_{\delta_w} \approx 0.26\cdot\frac{e^2 cZ_0 N}{\pi^{5/2} bE}\sqrt{\frac{M\ell}{\sigma_z}}, \qquad \frac{\sigma_z}{b} << 1 \qquad (19)$$

where b is the minimum radius of the bellows as shown in Figure 5.

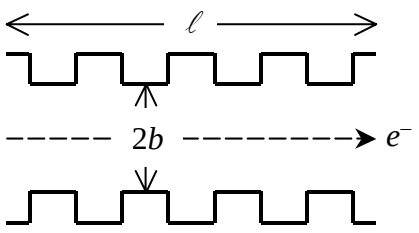

Figure 5. Cut-away view of a vacuum bellows with symbol definitions (M = 4 shown).

This diffraction model is valid for $b^2/2\sigma_z$ ($\approx$ 0.6 m) >> ℓ, and the emittance growth for n_b separate bellows is approximated by

$$\frac{\Delta\varepsilon_x}{\varepsilon_{x0}} \approx 0.033 \cdot \frac{n_b^2}{\pi^5}\left(\frac{e^2 c Z_0 N}{bE}\right)^2 \frac{M\ell}{\sigma_z}\theta^2 \frac{\beta_x}{\varepsilon_{x0}} << 1 \quad , \tag{20}$$

With two separate bellows between bend-3 and bend-4, each with M = 10 convolutions and ℓ = 0.1 m length (for a convolution period of 10 mm), and minimum full height of $2b$ = 30 mm, the emittance growth is 2.5 %. Bellows in other locations have even less effect due to the longer bunch length there. In any case, for two separate bellows between B3 and B4, it is advisable to keep the number of convolutions, and the bellows length to minimum values ($M \le 10$, $\ell \le 0.1$ m), while the bellows height is kept to a maximum ($2b \ge 30$ mm). The bellows might also be shielded by a smooth inner tube.

8.3 Radial 'Step-Out' Transitions

The rms relative energy spread induced by a sudden increase in vacuum chamber radius (*i.e.*, a radial 'step-out' transition) is [4]

$$\sigma_{\delta_w} \approx 0.11 \frac{e^2 Z_0 c N}{\pi E \sigma_z} \ln\left(\frac{b}{a}\right), \quad b \ge a, \quad \frac{\sigma_z}{a} << 1 \quad , \tag{21}$$

where a is the radius before, and b is the radius after the step-out. A 'step-in' transition generates no energy spread [4]. The effect on the emittance is overestimated for $(b - a)^2/\sigma_z > \Delta L$ (which is typical), so may be less significant than what is calculated here.

A step-out between B3 and B4, where the bunch length is almost fully compressed to 190 μm rms, generates an emittance growth of

$$\frac{\Delta\varepsilon_x}{\varepsilon_{x0}} \approx 6\times10^{-3} \cdot \left(\theta \frac{e^2 Z_0 c N}{\pi E \sigma_z} \ln\left(\frac{b}{a}\right)\right)^2 \frac{\beta_x}{\varepsilon_{x0}} << 1 \quad , \tag{22}$$

where β_x ($\approx$ 3.4 m) is evaluated at the center of B4. A step-out of $b/a \approx 2$ causes a 2% emittance growth, while a step-out of $b/a \approx 4$ causes a 8% growth. Vacuum chamber step-out transitions between B3 and B4 should be eliminated, or held to $b/a < 2$.

A step-out in the center of the chicane (between B2 and B3 where the bunch length is only half-compressed to $\sigma_z \approx 0.5$ mm) generates emittance growth $\Delta\varepsilon_x/\varepsilon_{x0} \approx 0.5\,\eta_{pk}^2\sigma_{\delta_w}^2\gamma_x/\varepsilon_{x0}$, or

$$\frac{\Delta\varepsilon_x}{\varepsilon_{x0}} \approx 6\times10^{-3}\cdot\left(\eta_{pk}\frac{e^2 Z_0 cN}{\pi E\sigma_z}\ln\left(\frac{b}{a}\right)\right)^2\frac{\gamma_x}{\varepsilon_{x0}} << 1 \quad , \tag{23}$$

where $\gamma_x \equiv (1 + \alpha_x^2)/\beta_x$ is evaluated after B4 ($\alpha_x \approx 0$, $\beta_x \approx 3.4$ m), and η_{pk} is the peak dispersion in the center of the chicane ($\eta_{pk} \approx 0.231$ m). A step-out here of $b/a \approx 4$ causes a 0.8% emittance growth. The BPM and profile monitor geometries should, therefore, avoid step-out transitions greater than $b/a \approx 4$ and a more careful wakefield analysis should be undertaken here. Step-out transitions between B1 and B2 are less of a problem.

8.4 Surface Roughness Wakefields

A tolerance on vacuum chamber interior surface finish is also set by the longitudinal wakefields of a rough surface [5]. If the B3-B4 chamber ($\Delta L \approx 2.435$ m) has a radius $a > 25$ mm, the beam is too far from the surface to be affected by it (*i.e.*, ($\Delta L << 2a^2/\sigma_z$)). The remaining important section is that of the narrow height B4-bend copper chamber ($2a \approx 30$ mm) which also is too short (*i.e.*, ($L_B << 2a^2/\sigma_z$)). Ignoring this just to calculate a conservative roughness requirement, the wakefield (V/C/m) generated by this section can be estimated using the treatment for a cylindrical chamber [5]

$$W(s) = \int_s^\infty \rho(s')\,w(s'-s)\,ds' \quad , \tag{24}$$

where ρ is the line-charge distribution, and w is the point-charge wake function given by

$$w(\zeta) = \frac{h^2\kappa^{3/2}}{2\sqrt{\pi}\,a}\frac{\partial}{\partial\zeta}\frac{1}{\sqrt{\zeta}}\left(\cos\frac{\kappa\zeta}{2} + \sin\frac{\kappa\zeta}{2}\right) \quad . \tag{25}$$

Here h is the peak surface roughness in the radial direction (rms surface finish $h_{rms} \approx h/\sqrt{2}$), and $\kappa \equiv 2\pi/\lambda$, with λ as the typical roughness bump length (in beam direction). Equation (23) is integrated by parts in order to avoid the singularity at high frequencies where $s' \to s$.

The wakefield-induced relative energy loss and rms spread is evaluated in Figure 6 using a Gaussian bunch with $\sigma_z = 190\ \mu$m, $\lambda = 50\ \mu$m, $N = 6.2\times10^9$, $L/2 = 0.1$ m, $E_0 = 250$ MeV, $h_{rms} = 10\ \mu$m, $a = 15$ mm. The mean relative energy loss is 2×10^{-7} and the rms spread is 2.3×10^{-5}, which is just tolerable. However, this 10-μm roughness requirement should not be difficult to achieve, were it necessary.

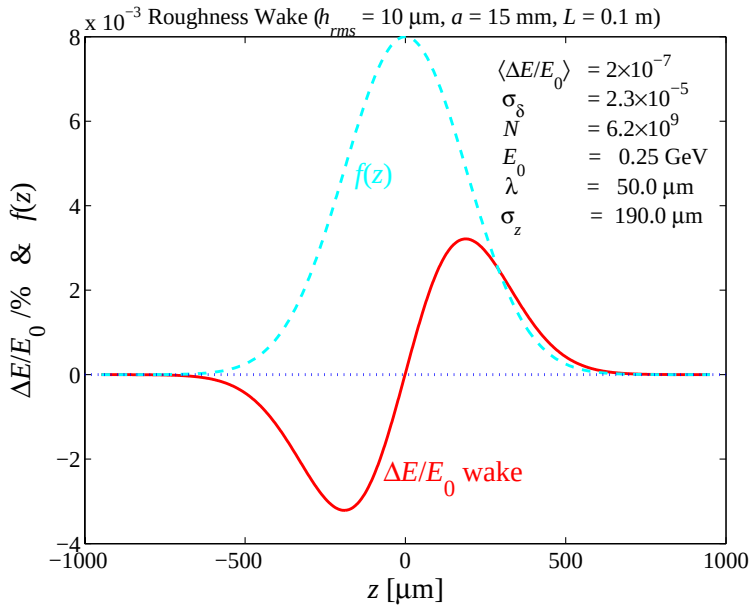

Figure 6. Surface roughness wakefield (solid-red) over Gaussian bunch with $\sigma_z = 190\ \mu$m, $\lambda = 50\ \mu$m, $N = 6.2\times10^9$, $L/2 = 0.1$ m, $E_0 = 250$ MeV, $h_{rms} = 10\ \mu$m, $r = 15$ mm. The mean relative energy loss is 2×10^{-7} and the rms spread is 2.3×10^{-5}.

The length, $L/2 = 0.1$ m, is taken as the half-length of the B4 chamber, treating the bend as a thin kick at the bend center. In this case, a 10-μm rms bump size with a 50-μm bump length generates enough energy spread to cause a 0.3% emittance growth. This should be taken as the conservative surface finish tolerances for the B4 chamber. Larger a, longer λ, and/or smaller h is better, but not necessary.

8.5 Coherent Synchrotron Radiation

The effects of coherent synchrotron radiation (CSR) can be shielded if the full vacuum chamber height, $2a$, is much smaller than

$$2a < \frac{1}{2}\left(\pi\sigma_z\sqrt{\frac{L_B}{|\theta|}}\right)^{2/3} \approx 4 \text{ mm} \qquad (26)$$

.

This is too small to realistically use, especially since the resistive-wall wakefields may increase to intolerable levels. CSR-shielding will, therefore, not be employed, and the vacuum chamber height will be set by the resistive-wall or other limits described above.

The effects of unshielded CSR have been estimated by particle tracking from the damping rings through the BC1 chicane. The field transients and bend-to-bend drift contributions have been included using a line-charge model taken from reference [6] and generalizations added by G. Stupakov and P. Emma [7]. At $N = 6.2\times10^9$, the emittance growth due to CSR is 4% (with an initial emittance of $\gamma\varepsilon_{x_0} = 1$ μm). This is further reduced to 2% if the linear dispersion is adjusted with the CQ11/CQ12 tuning quads. In this case, the input beta functions at B1 entrance are $\beta \approx 16.2$ m and $\alpha_x \approx 2.0$ (as shown in Figure 3). The CSR-induced relative energy loss and rms spread along the chicane are shown in Figure 7, while the longitudinal phase space and the energy and 'temporal' distributions at end of chicane are shown in Figure 8 at 250 MeV, with the CSR-induced wakefield energy gradient along the bunch plotted at lower right.

The average coherent power radiated by the bunch in the chicane is given by the CSR energy loss ($\Delta E/E_0 \approx 0.07\%$, or $\Delta E \approx 175$ keV per electron, shown in Fig. 7) multiplied by the machine repetition rate, f (= 120 Hz). The power absorbed by the vacuum chamber is negligible: $P \approx \Delta E f N \approx 0.02$ watts.

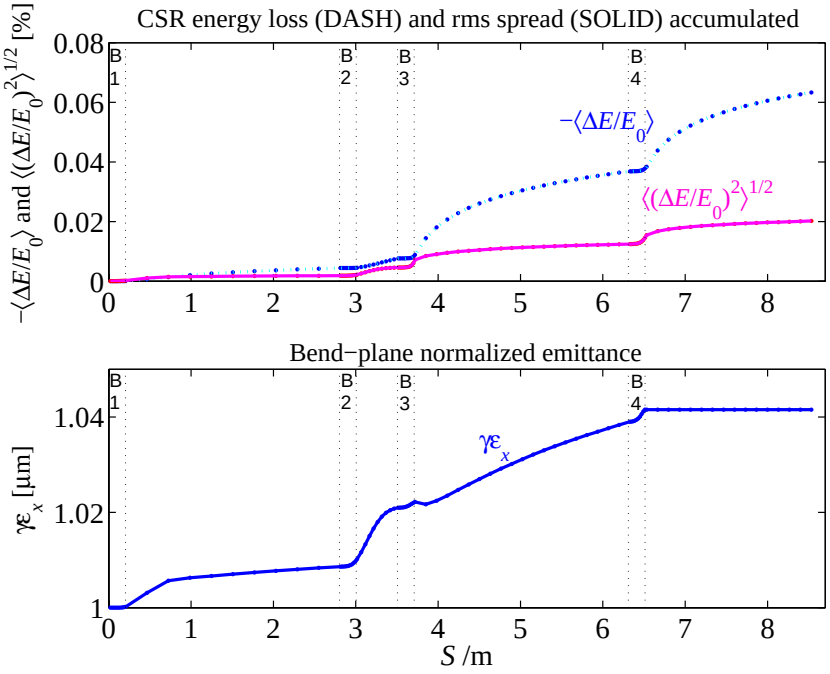

Figure 7. CSR-induced energy loss (dash) and rms energy spread (solid) along chicane at 250 MeV.

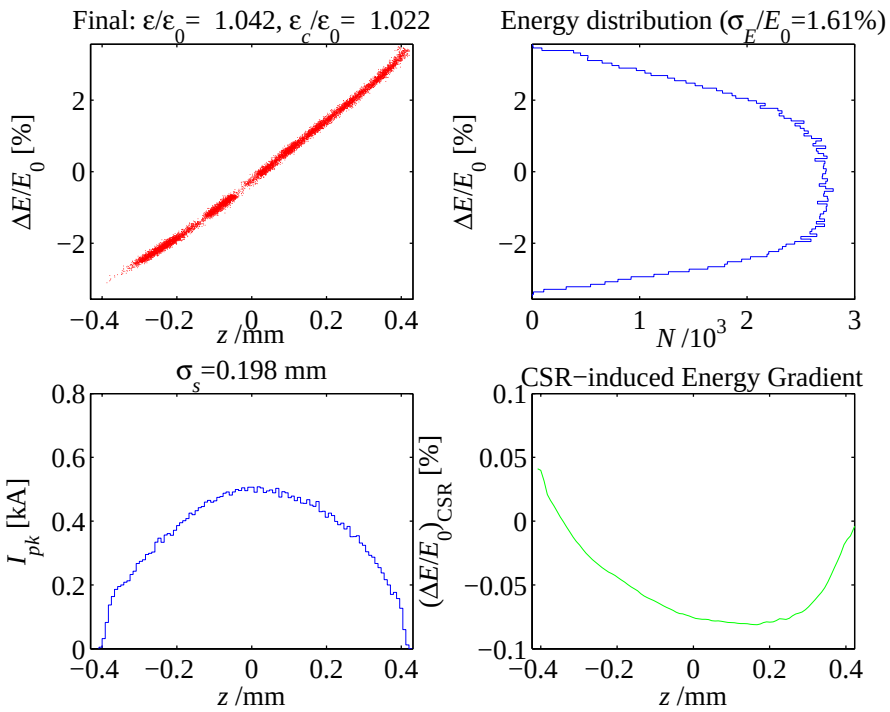

Figure 8. Longitudinal phase space with energy and 'temporal' distributions at end of chicane at 250 MeV. The net CSR-induced wakefield energy gradient is shown at lower right (bunch head at left).

8.6 Vacuum Chamber Summary

Table 4 summarizes the vacuum chamber requirements set by wakefield effects.

Table 4. Vacuum chamber limits based on wakefield effects.

parameter	**symbol**	**value**	**unit**
Vacuum chamber minimum full-height	$2a$	30	mm
Minimum full-width inside bends	w	0.10	m
Number of bellows allowed (B1-B2)		3	
Number of bellows allowed (B2-B3)		2	
Number of bellows allowed (B3-B4)		2	
Maximum length of each bellows	ℓ	0.1	m
Maximum convolutions per bellows	M	10	
Minimum full-height of bellows	$2b$	30	mm
Maximum ×2 step-out transitions (B3-B4)		1	

9 Summary

The various BC1 chicane tolerances and specifications are listed in the four tables above.

10 References

[1] T. O. Raubenheimer et al., "Chicane and Wiggler Based Bunch Compressors for Future Linear Colliders," SLAC-PUB-6119, May 1993.

[2] K.L.F. Bane, M. Sands, "The Short-Range Resistive Wall Wakefields," Contributed *to Micro Bunches: A Workshop on the Production, Measurement and Applications of Short Bunches of Electrons and Positrons in Linacs and Storage Rings*, Upton, New York, September 28-30, 1995.

[3] K.L.F. Bane, M. Sands, "Wakefields of Very Short Bunches in an Accelerating Cavity", *Particle Accelerators*, Vol. 25, pp. 73-95, (1990).

[4] S. A. Kheifets, IEEE Trans. Microwave Technique MTT-35, 753-760 (1987).

[5] G. Stupakov, "Surface Roughness Impedance", *Physics of, and Science with, the X-ray Free Electron Laser*, Sep. 2000, Arcidosso, Italy.

[6] E. L. Saldin, et. al., TESLA-FEL-96-14, Nov. 1996.

[7] G. Stupakov, P. Emma, in Proc. of EPAC'02, Paris France, 2002, p. 1479.